



Sensitivity and constraints to the 2HDM soft-breaking Z_2 parameter m_{12}

F. Arco^{a,b,*}, S. Heinemeyer^b, M.J. Herrero^{a,b}

^a Departamento de Física Teórica and Instituto de Física Teórica, Universidad Autónoma de Madrid, Cantoblanco, 28049 Madrid, Spain

^b Instituto de Física Teórica, IFT-UAM/CSIC, Universidad Autónoma de Madrid, Cantoblanco, 28049 Madrid, Spain

ARTICLE INFO

Article history:

Received 3 August 2022

Received in revised form 25 October 2022

Accepted 3 November 2022

Available online 4 November 2022

Editor: A. Ringwald

ABSTRACT

In this letter we study the specific sensitivity and constraints to the soft breaking Z_2 parameter m_{12} of the Two Higgs Doublet Model (2HDM). m_{12} is considered here as an input parameter of the model together with the masses of the Higgs bosons, m_h , m_H , m_A , m_{H^\pm} , the ratio of the two Higgs vacuum expectation values, $\tan\beta$, and $\cos(\beta - \alpha)$, with α and β the mixing angles of the \mathcal{CP} -even and \mathcal{CP} -odd Higgs sector, respectively. We explore in particular the sensitivity to m_{12} in the decays of the lightest Higgs boson h to two photons, assuming: 1) that h is the state observed at the LHC at ~ 125 GeV, and 2) the h couplings to the SM particles are SM-like, by going to the alignment limit, $\cos(\beta - \alpha) = 0$. The aim of this work is to demonstrate possible constraints on m_{12} from the present measurement of the di-photon signal strength, $\mu_{\gamma\gamma}$. These constraints are relevant in the region of the 2HDM parameter space that is allowed by all the other constraints, specifically, theoretical constraints as well as experimental constraints from LHC Higgs rate measurements, Higgs boson searches, flavor physics and precision observables. The exploration is performed in the four different Yukawa types of 2HDM, where the allowed region by all the other constraints depends on the model type. We also analyze the case that the Higgs-boson mass spectrum accommodates a possible new world average of m_W including the recent CDF measurement.

© 2022 The Authors. Published by Elsevier B.V. This is an open access article under the CC BY license (<http://creativecommons.org/licenses/by/4.0/>). Funded by SCOAP³.

1. Introduction

The Two Higgs Doublet Model (2HDM) is one of the most studied extensions of the Standard Model (SM) of particle physics, and it has been explored exhaustively for many years (see, e.g., [1–3] for reviews). This model contains two Higgs doublets, Φ_1 and Φ_2 , that accommodate the five physical Higgs bosons: the two \mathcal{CP} -even h and H , the \mathcal{CP} -odd A , and the pair of charged Higgs bosons, H^\pm . The lightest Higgs boson h is usually assumed to be SM-like with a mass set to the experimentally measured value of ~ 125 GeV (see, e.g., [4], for a recent summary). Other parameters are the two mixing angles α and β which diagonalize the \mathcal{CP} -even and \mathcal{CP} -odd Higgs boson sector, respectively, and $\tan\beta = v_2/v_1$, the ratio of the two Higgs vacuum expectation values, which are related to the SM vev by $v = \sqrt{v_1^2 + v_2^2}$.

In order to avoid flavor changing neutral currents (FCNC) at the tree-level, a Z_2 symmetry is imposed [5]. When this symmetry is

allowed to be softly broken in the Higgs potential, an extra 2HDM parameter m_{12} with dimension of mass is included in the Higgs potential by a new term $\sim m_{12}^2(\Phi_1^\dagger\Phi_2 + \Phi_2^\dagger\Phi_1)$. The relevance of this m_{12} parameter is clear, since it provides the mixing between the two Higgs doublets which in turn can give rise to FCNC beyond the tree level. Therefore limiting the size of this m_{12} parameter is a very important issue, complementing constraining the physical Higgs boson masses.

Four types of the 2HDM can then be realized, depending on how this Z_2 symmetry is implemented into the fermion sector: types I–IV [2]. Once m_h and v are set to $m_h \simeq 125$ GeV and $v \simeq 246$ GeV, the four 2HDM types can be fully described in terms of six input parameters which we choose here to be: $\cos(\beta - \alpha)$, $\tan\beta$, m_H , m_A , m_{H^\pm} and m_{12} .

So far, the experimental searches for these new Higgs bosons have not found any indication of their existence, neither direct nor indirect, setting limits on the 2HDM parameters. There are many analyses in the literature of these constraints, including various sets of data, various choices of benchmark planes, and various ways to implement the theoretical constraints on these parameters (considering, for instance, a tree-level or one-loop analysis). We will focus here on the analysis of the 2HDM constraints presented

* Corresponding author.

E-mail addresses: francisco.arco@uam.es (F. Arco), Sven.Heinemeyer@cern.ch (S. Heinemeyer), maria.herrero@uam.es (M.J. Herrero).

in Ref. [6], which has been recently updated to the four types of 2HDM in Ref. [7]. This analysis was performed with the goal of deriving the allowed ranges of the triple Higgs boson coupling. These couplings can have interesting consequences for the double Higgs production at e^+e^- colliders, as it was shown in Ref. [8]. Notice that with our choice of input parameters, and using the physical basis, these triple Higgs couplings $\lambda_{h_i h_j h_k}$ are derived quantities, and it was demonstrated in Refs. [6,7] that some of them can reach sizeable values. In particular, it was shown in Ref. [7] that the coupling of the lightest Higgs to the charged Higgs bosons $\lambda_{hH^+H^-}$ can be as large as $\sim 20 - 30$, in the four 2HDM types and yet be compatible with all the present constraints.

Our main motivation in this letter is to perform a dedicated study on the sensitivity to the soft-breaking Z_2 parameter m_{12} in order to analyze the constraints on this parameter. In this analysis we will include all available theoretical and experimental constraints on equal footing for the four 2HDM Yukawa types, following the same procedure as in Ref. [7]. The most important difference with respect to our previous analysis is that here, in addition to the full set of constraints specified in Ref. [7], we will select and analyze in full detail one particular observable which carries the highest sensitivity to the m_{12} parameter. This observable is the decay width of the lightest Higgs boson to two photons, $\Gamma(h \rightarrow \gamma\gamma)$ that proceeds in the 2HDM at the one-loop level. The prediction of this partial width within the SM is known since long ago [9]. Additional contributions from charged scalars are also known since long ago [10] (see also Ref. [1] for a review). The sensitivity to m_{12} occurs via the charged Higgs boson loop and precisely through the triple Higgs coupling $\lambda_{hH^+H^-}$. Our goal here is to determine and update the sensitivity to m_{12} via the prediction of the ratio $\text{BR}(h \rightarrow \gamma\gamma)$ in the 2HDM, and conclude on the corresponding constraints to m_{12} from the comparison with the present experimental signal strength $\mu_{\gamma\gamma}$ [4]. Another important difference in the present analysis with respect to Ref. [7] is that we restrict ourselves here to the alignment limit [11] where $\cos(\beta - \alpha) \rightarrow 0$. This limit is in very good agreement with the present data from LHC rate measurements, that restrict the size of $\cos(\beta - \alpha)$ to values lower than $\mathcal{O}(10^{-2})$ for type II and III and lower than $\mathcal{O}(10^{-1})$ for type I and IV, see for instance Refs. [6,7]. In the alignment limit the h couplings to SM particles approach the corresponding SM couplings. However, there are important implications for beyond SM physics from the triple Higgs couplings of h to the heavy Higgs bosons, and here in particular from $\lambda_{hH^+H^-}$, which carries the sensitivity to m_{12} via the $h \rightarrow \gamma\gamma$ decay.

2. The m_{12} soft-breaking parameter in the 2HDM

The m_{12} soft-breaking parameter appears in the Higgs potential of the 2HDM. This potential for the \mathcal{CP} conserving 2HDM is given in terms of eight parameters by [3]:

$$V = m_{11}^2(\Phi_1^\dagger \Phi_1) + m_{22}^2(\Phi_2^\dagger \Phi_2) - m_{12}^2(\Phi_1^\dagger \Phi_2 + \Phi_2^\dagger \Phi_1) + \frac{\lambda_1}{2}(\Phi_1^\dagger \Phi_1)^2 + \frac{\lambda_2}{2}(\Phi_2^\dagger \Phi_2)^2 + \lambda_3(\Phi_1^\dagger \Phi_1)(\Phi_2^\dagger \Phi_2) + \lambda_4(\Phi_1^\dagger \Phi_2)(\Phi_2^\dagger \Phi_1) + \frac{\lambda_5}{2}[(\Phi_1^\dagger \Phi_2)^2 + (\Phi_2^\dagger \Phi_1)^2], \quad (1)$$

where Φ_1 and Φ_2 denote the two $SU(2)_L$ scalar doublets. As mentioned above, the occurrence of tree-level flavor changing neutral currents (FCNC) is avoided by imposing a Z_2 symmetry on the scalar potential. The scalar fields transform as $\Phi_1 \rightarrow \Phi_1$, $\Phi_2 \rightarrow -\Phi_2$. The Z_2 symmetry, however, is softly broken by the m_{12}^2 term in the Lagrangian. The extension of the Z_2 symmetry to the Yukawa sector avoids tree-level FCNCs.

Depending on the Z_2 parities of the fermions, this results in four variants of 2HDM: type I, type II, type III (also known as

Table 1

Allowed fermion couplings in the four 2HDM types.

	u-type	d-type	leptons
Type I	Φ_2	Φ_2	Φ_2
Type II	Φ_2	Φ_1	Φ_1
Type III	Φ_2	Φ_1	Φ_2
Type IV	Φ_2	Φ_2	Φ_1

type Y or flipped) and type IV (also known as type X or lepton-specific) [2], that are summarized in Table 1.

After the consideration of the minimization conditions of the above potential for the implementation of the electroweak symmetry breaking (with $v \simeq 246$ GeV), using the physical basis for the Higgs sector and identifying the lightest \mathcal{CP} -even Higgs boson, h , with the one observed at ~ 125 GeV, the free parameters of the 2HDM are reduced to the following six:

$$c_{\beta-\alpha}, \tan \beta, m_H, m_A, m_{H^\pm}, m_{12}. \quad (2)$$

Here and from now on we use the short-hand notation $s_x = \sin(x)$, $c_x = \cos(x)$.

The triple Higgs couplings in the physical basis, $\lambda_{h_i h_j h_k}$, are then derived quantities that can be evaluated from the input parameters in Eq. (2). We employ here the tree level predictions for these triple couplings whose specific expressions and notation are taken from Refs. [6,7]. In particular, the triple coupling of the lightest Higgs boson to the charged Higgs bosons is given by:

$$\lambda_{hH^+H^-} = \frac{1}{v^2} \left\{ (m_h^2 + 2m_{H^\pm}^2 - 2\bar{m}^2) s_{\beta-\alpha} + 2 \cot 2\beta (m_h^2 - \bar{m}^2) c_{\beta-\alpha} \right\}, \quad (3)$$

where the soft-breaking parameter m_{12} enters via \bar{m} , which is defined by:

$$\bar{m}^2 = \frac{m_{12}^2}{\sin \beta \cos \beta}. \quad (4)$$

The introduction of this auxiliary parameter \bar{m} in the present analysis is convenient for practical reasons, and because it summarizes the effect of m_{12} and $\tan \beta$ in $\lambda_{hH^+H^-}$. Finally, when assuming the alignment limit, the triple coupling $\lambda_{hH^+H^-}$ simplifies to:

$$\lambda_{hH^+H^-}^{\text{align}} = \frac{1}{v^2} (m_h^2 + 2m_{H^\pm}^2 - 2\bar{m}^2). \quad (5)$$

Therefore, the size of this relevant triple coupling is directly related to the splitting ($m_{H^\pm}^2 - \bar{m}^2$).

3. $h \rightarrow \gamma\gamma$ in the alignment limit: sensitivity to m_{12}

As it is well known, the di-photon decay of the neutral Higgs boson h proceeds at the one-loop level with contributions from fermions, W bosons, and charged Higgs bosons. The partial width $\Gamma(h \rightarrow \gamma\gamma)$ was computed long ago [9], and it is usually written in terms of the corresponding form factors for the fermion, A^f , W boson, A^{W^\pm} , and charged Higgs boson loop contributions, A^{H^\pm} . Generically (see, for instance, the full formula in [1,12]) it can be written as:

$$\Gamma(h \rightarrow \gamma\gamma) = \frac{\alpha^2 m_h^3}{256 \pi^3 v^2} |A^f + A^{W^\pm} + A^{H^\pm}|^2. \quad (6)$$

The prediction for this partial width in the 2HDM is in general different from the SM Higgs di-photon width. However, in the alignment limit, the only difference between the 2HDM and the SM prediction comes from the contribution of the charged Higgs

boson loops, where the corresponding contribution can be written as:

$$A^{H^\pm} = -\lambda_{hH^+H^-}^{\text{align}} \frac{v^2}{2m_{H^\pm}^2} F_0(\tau_{H^\pm}), \quad (7)$$

where, $\tau_{H^\pm} = m_h^2/(4m_{H^\pm}^2)$, and

$$F_0(\tau) = \tau^{-1} \left(\tau^{-1} \arcsin^2(\sqrt{\tau}) - 1 \right). \quad (8)$$

Therefore, the relevant parameters that will give the main differences between the 2HDM prediction of $\Gamma(h \rightarrow \gamma\gamma)$ in the alignment limit with respect to the SM prediction are clearly, m_{H^\pm} , m_{12} and $\tan\beta$. The sensitivity to m_{12} and $\tan\beta$ in the partial width comes jointly from the \bar{m} that appears in $\lambda_{hH^+H^-}$ which, as discussed above, is a derived parameter.¹ Notice that the other 2HDM mass parameters, m_H and m_A , do not enter at leading order in the partial width $\Gamma(h \rightarrow \gamma\gamma)$, or in the total h width as long as the alignment limit is imposed, no EW higher order corrections are included, and the decay channel $h \rightarrow AA$ is not kinematically open. In our analysis for the numerical evaluations of the $\text{BR}(h \rightarrow \gamma\gamma)$ we use the code 2HDMC-1.8.0 [12].

The main aspects of the sensitivity to m_{12} in $\text{BR}(h \rightarrow \gamma\gamma)$ are summarized in Fig. 1. In the upper row we show the m_{12} - m_{H^\pm} plane (left) and the m_{12} - $\tan\beta$ plane (right) for $m_H = m_A = m_{H^\pm}$ with $\tan\beta = 3$ (left) and $m_{H^\pm} = 550$ GeV (right). The color coding indicates $\text{BR}(h \rightarrow \gamma\gamma)$. The blue line indicates the “SM limit”, which we define here by setting the input m_{12} such that $\lambda_{hH^+H^-} = 0$. One can observe that for fixed $m_{H^\pm} > 200$ GeV and $\tan\beta > 1$, the BR grows with m_{12} and gets values clearly above the SM value in a large region of the 2HDM parameter space.

In the middle row we show $\text{BR}(h \rightarrow \gamma\gamma)$ as a function of m_{H^\pm} for $\tan\beta = 1$ (left) and $\tan\beta = 50$ (right) for various choices of m_{12} , where the “SM limit” is represented by the horizontal blue lines. One can observe that for fixed m_{12} (solid lines) the coincidence of the 2HDM prediction with the SM value does not occur in the very heavy charged Higgs-boson limit where $m_{H^\pm} \rightarrow \infty$, since $\lambda_{hH^+H^-}$ being a derived quantity grows with m_{H^\pm} , (and at some point becomes non-perturbative), and as a consequence the $\text{BR}(h \rightarrow \gamma\gamma)$ tends to a constant value different than the SM value. In this heavy charged Higgs-boson limit the loops with charged Higgs bosons are not really decoupled. In fact, $A^{H^\pm} \rightarrow -1/3$ in the limit $m_{H^\pm} \rightarrow \infty$. On the other hand, in a different setting of the input parameters with $m_{H^\pm} = \bar{m}$ (dashed olive lines) the triple Higgs coupling $\lambda_{hH^+H^-}^{\text{align}}$ takes a fixed value of m_h^2/v^2 (see Eq. (5)) and, for $m_{H^\pm} \rightarrow \infty$, the $\text{BR}(h \rightarrow \gamma\gamma)$ tends to the same constant value as the above defined “SM limit”. Therefore, in summary, to quantify the sensitivity to m_{12} in $\text{BR}(h \rightarrow \gamma\gamma)$ the optimal comparison is to estimate the departure of the 2HDM prediction with respect to the “SM limit” defined in this section. The concrete value that we obtain for $\text{BR}(h \rightarrow \gamma\gamma)$ in this is “SM limit” is 2.181×10^{-3} .

Finally, in the lower left plot of Fig. 1 the prediction of $\text{BR}(h \rightarrow \gamma\gamma)$ is shown in the $(\bar{m}$ - $m_{H^\pm})$ plane, as before also in the alignment limit. For comparison in the lower right plot we show the prediction for $\text{BR}(h \rightarrow Z\gamma)$ for the same choice of parameters. In the upper axes of these two plots the corresponding m_{12} values for $\tan\beta = 2$ are displayed. The SM limit contours indicated by the blue lines where $\lambda_{hH^+H^-} = 0$ are included as well. The dependence on $\tan\beta$ and m_{12} in both cases enters through the parameter \bar{m} present in $\lambda_{hH^+H^-}$. Consequently, as expected, both observables $\text{BR}(h \rightarrow \gamma\gamma)$ and $\text{BR}(h \rightarrow Z\gamma)$ display similar dependences on the relevant parameters m_{H^\pm} , $\tan\beta$ and m_{12} . The dashed red lines in

these two plots indicate the current 95% CL limits that are extracted from the corresponding signal strengths (which will be discussed in detail in the next section). In the $\gamma\gamma$ channel the allowed area lies inside the two dashed red lines. In the γZ channel the allowed area covers practically the full (\bar{m}, m_{H^\pm}) plane shown, except for very low values of $m_{H^\pm} \lesssim 200$ GeV in the lower right corner. From these plots one can read off that in the allowed area for $\text{BR}(h \rightarrow \gamma\gamma)$ the predictions for $\text{BR}(h \rightarrow Z\gamma)$ give values in the interval $1.43 \times 10^{-3} - 1.58 \times 10^{-3}$, which are far from the present sensitivity. This demonstrates that $\text{BR}(h \rightarrow \gamma\gamma)$ is by far the most constraining observable for m_{12} , and thus it will be the focus of this letter.

4. Summary of the applied constraints

We summarize here the experimental and theoretical constraints on the 2HDM parameters that are considered in the present analysis (more details can be found in Refs. [6,7]).

• Constraints from electroweak precision data

Constraints from the electroweak precision observables (EWPO) can for “pure” Higgs-sector extensions of the SM, be expressed in terms of the oblique parameters S , T and U [14,15]. Previous explorations of these parameters within the 2HDM were done long ago, see for instance [16,17]. In the 2HDM the T parameter is the most constraining parameter and requires either $m_{H^\pm} \approx m_A$ or $m_{H^\pm} \approx m_H$. For the numerical evaluation of the S , T and U parameters in the 2HDM we use the code 2HDMC-1.8.0 [12] where the one-loop formulas are implemented. These numerical predictions for S , T and U are compared with the experimental allowed values which we take from [4]. These constraints so far do not take into account the recent measurement of m_W by CDF [18]. However, below we also analyze the case of a possible new world average of m_W , where this measurement is included.

• Theoretical constraints

Here the important constraints come from tree-level perturbative unitarity and stability of the vacuum. They are ensured by an explicit test on the underlying Lagrangian parameters, see Ref. [6] for details. For the evaluation of these theoretical constraints we use our private code in which we have implemented the formulas of the review [19] (see also references therein, where the original computations can be found), following the procedure described in Ref. [6].

• Constraints from searches for BSM Higgs bosons

The 95% confidence level exclusion limits of all relevant searches for BSM Higgs bosons are included in the public code HiggsBounds v.5.9 [20,21], including Run 2 data from the LHC. To test a (2HDM) parameter point, based on the masses, partial widths etc. of the Higgs bosons in the model, HiggsBounds (HB) determines which is the most sensitive channel based on the expected experimental limits. Only this limit is then used to test whether a Higgs boson is allowed or not at the 95% CL. The required input is calculated with the help of 2HDMC [12].

• Constraints from the LHC Higgs rate measurements

Any model beyond the SM has to accommodate the SM-like Higgs boson, with mass and signal strengths as they were measured at the LHC. In our scans the compatibility of the \mathcal{CP} -even scalar h with a mass of 125.09 GeV with the measurements of LHC rate measurements is checked with the code HiggsSignals v.2.6 [22,23] (HS). The code provides a statistical χ^2 analysis, where the various measured LHC signal rates are compared with the model prediction for the parameter point under consideration. Again, the predictions of the 2HDM have been obtained with 2HDMC [12]. As in Ref. [6,7],

¹ The sensitivity to the λ_5 coupling of the potential (which is related to \bar{m}) in $h \rightarrow \gamma\gamma$ decays and in the alignment limit was also studied previously in [13] reaching similar conclusions on the effects of this parameter on the $\text{BR}(h \rightarrow \gamma\gamma)$.

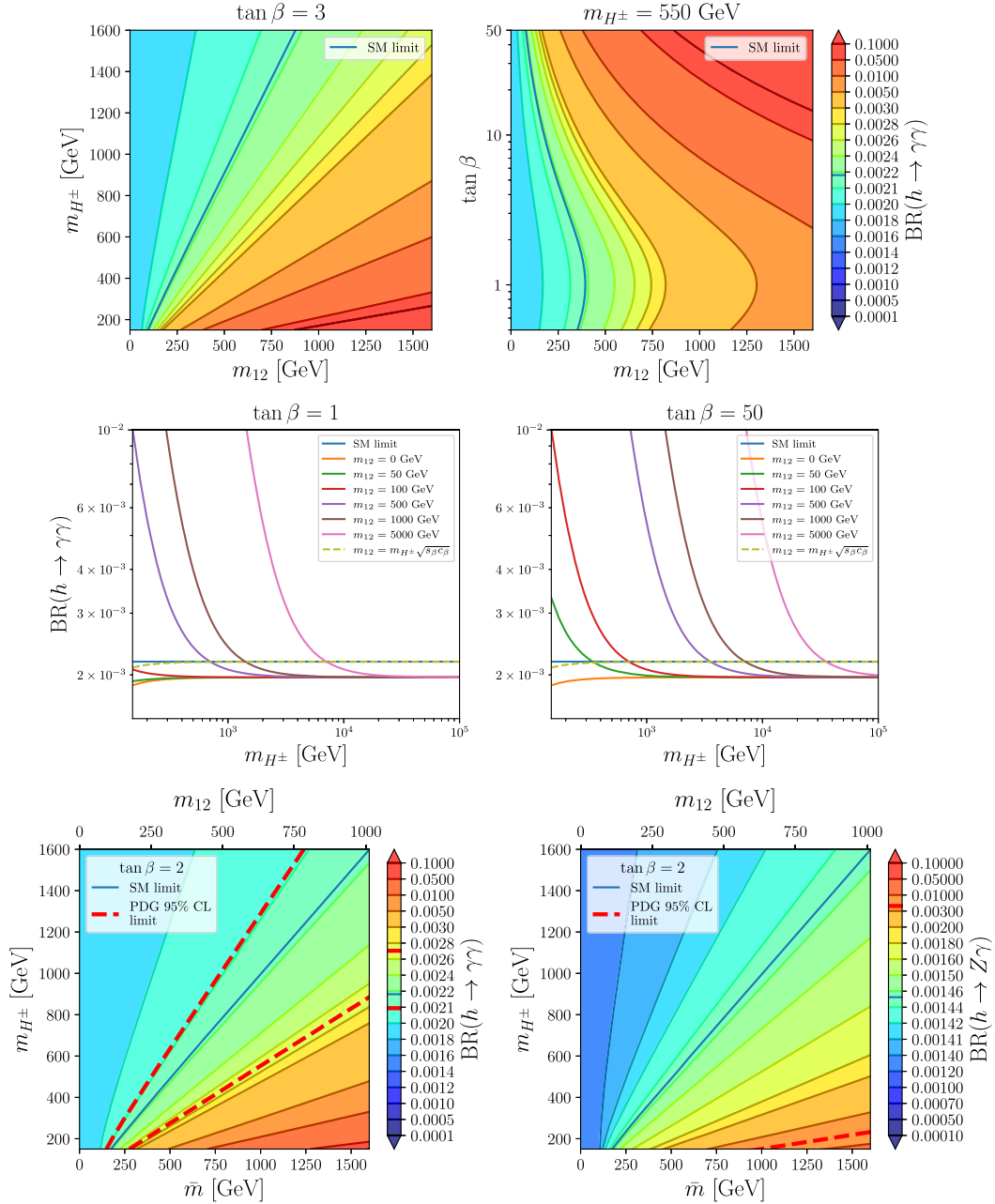


Fig. 1. $\text{BR}(h \rightarrow \gamma\gamma)$ in the 2HDM, in the alignment limit, as a function of the relevant parameters m_{H^\pm} , $\tan \beta$ and m_{12} (upper and middle rows). In the lower row we compare the prediction for $\text{BR}(h \rightarrow \gamma\gamma)$ (left) to the prediction for $\text{BR}(h \rightarrow Z\gamma)$ (right) in the (\bar{m}, m_{H^\pm}) plane.

we require that for a parameter point of the 2HDM to be allowed, the corresponding χ^2 is within 2σ ($\Delta\chi^2 = 6.18$) from the SM value.

• Constraints from flavor physics

Constraints from flavor physics have proven to be very significant in the 2HDM mainly because of the presence of the charged Higgs boson. Various flavor observables like rare B decays, B meson mixing parameters, $\text{BR}(B \rightarrow X_s \gamma)$, LEP constraints on Z decay partial widths etc., which are sensitive to charged Higgs boson exchange, provide effective constraints on the available parameter space [24,25]. Other observables like $\tau \rightarrow \mu \nu \nu$ have also been considered in the literature [24,26]. However, this τ decay is only relevant in type IV (lepton-specific) at very low values of $m_{H^\pm} < 200$ GeV, very low values of $m_A < 100$ GeV and very large $\tan \beta$ above 40. Here we take into account the decays $B \rightarrow X_s \gamma$ and $B_s \rightarrow \mu^+ \mu^-$,

which are most constraining. This is done with the code *SuperIso* [27,28] where the model input is given by 2HDMC. It should be noted that *SuperIso* does not implement the recent improved calculation of $\text{BR}(B \rightarrow X_s \gamma)$ within the 2HDM in Ref. [29], where a better lower bound of ~ 800 GeV for m_{H^\pm} in the 2HDM type II is quoted (which should also apply in type III). However, at present there is some open discussion on the size of the theoretical uncertainties involved on this calculation and we have preferred to use the older computation implemented in *SuperIso*. We have also modified the code as to include the Higgs-Penguin type corrections in $B_s \rightarrow \mu^+ \mu^-$ (we use the formulas in [30]) which were not included in the original version of *SuperIso*. These corrections are indeed relevant for the present work since these Higgs-Penguin contributions are the ones containing the potential effects from triple Higgs couplings in $B_s \rightarrow \mu^+ \mu^-$.

• Specific constraints on m_{12}

In the alignment limit that we are assuming through this work, the most relevant restrictions to m_{12} are those from the theoretical constraints previously commented and from the experimental constraints to $\text{BR}(h \rightarrow \gamma\gamma)$. The other sensitive observable to m_{12} is $\text{BR}(B_s \rightarrow \mu^+\mu^-)$ but this sensitivity is very mild and only emerges at extremely high $\tan\beta$ values, larger than 50 [6,7], which we do not consider here. (For the results shown below there is no visible impact). Furthermore, the constraint on m_{12} from $\text{BR}(B_s \rightarrow \mu^+\mu^-)$ applies exclusively in the type II models as it has been discussed in Ref. [6]. Another observable that could be sensitive to m_{12} is $\text{BR}(h \rightarrow Z\gamma)$. As we have seen in the previous section, in the alignment limit, it depends only on m_{H^\pm} , $\tan\beta$ and m_{12} as the $\text{BR}(h \rightarrow \gamma\gamma)$. However, the sensitivity to m_{12} is milder in the $Z\gamma$ channel than in the $\gamma\gamma$ channel because the experimental bound to the signal strength is $\mu_{Z\gamma} < 3.6$ at 95% CL [4], much less precise than the one in the $\gamma\gamma$ case. The predictions in the 2HDM of this observable in the parameter space explored in this paper would only exclude the low m_{H^\pm} region with $m_{H^\pm} < 200$ GeV, corresponding to values of $\text{BR}(h \rightarrow Z\gamma) > 5 \times 10^{-3}$, as can be observed in the lower right plot in Fig. 1. It should also be noted that the S , T and U parameters considered here at one loop are not sensitive to m_{12} . However, this sensitivity might change in a two loop computation. According to Ref. [31], this sensitivity (given in terms of λ_5 in that reference) is very mild and it only appears at very low $\tan\beta$ values < 1 (see for instance Fig. 3 in that reference), which on the other hand are already strongly restricted by flavor physics. Hence, we have preferred to use here the one loop formulas implemented in the 2HDMC to study the oblique parameters. Overall, we then pay attention here to the specific analysis of m_{12} from the two most restricting requirements: the theoretical ones and the experimental constraints on $\text{BR}(h \rightarrow \gamma\gamma)$. To apply the latter we compare the prediction of $\text{BR}(h \rightarrow \gamma\gamma)$ within the 2HDM in the alignment limit with the experimentally measured value. The experimental data, as averaged in Ref. [4], is given by

$$\mu_{\gamma\gamma}^{\text{exp}} = \frac{\sigma(pp \rightarrow h)_{\text{exp}} \text{BR}(h \rightarrow \gamma\gamma)_{\text{exp}}}{\sigma(pp \rightarrow h)_{\text{SM}} \text{BR}(h \rightarrow \gamma\gamma)_{\text{SM}}} = 1.10 \pm 0.07. \quad (9)$$

Here $\text{BR}(h \rightarrow \gamma\gamma)_{\text{SM}}$ denotes the “SM limit” as defined above. This can readily be compared to the theory prediction by:

$$\mu_{\gamma\gamma}^{\text{2HDM}} = \frac{\text{BR}(h \rightarrow \gamma\gamma)_{\text{2HDM}}}{\text{BR}(h \rightarrow \gamma\gamma)_{\text{SM}}}. \quad (10)$$

Notice that in the alignment limit, the ratio of the production cross section of h respect to the SM present in the definition of the signal strength cancels and $\mu_{\gamma\gamma}$ is then given just in terms of the BRs.

The main difference of the analysis presented below with respect to the ones in Refs. [6,7] is that we focus now on the alignment limit (which we did not in our previous works) and that the $\mu_{\gamma\gamma}$ is imposed *separately* as a specific constraint on m_{12} (and not only in the sum of all LHC rate measurements). This choice is justified, since we are investigating the possible restrictions on m_{12} , and $\text{BR}(h \rightarrow \gamma\gamma)$ is effectively the only sensitive quantity to m_{12} . Just looking at the overall LHC rate measurement would dilute this sensitivity. As discussed above, we first apply constraints from theory, EWPO, colliders, and flavor observables, from now on called “other constraints”. In the final step we will apply the constraints of $\text{BR}(h \rightarrow \gamma\gamma)$ and conclude on the m_{12} values that are

allowed by these other constraints, but disallowed by $\mu_{\gamma\gamma}$. Since these other constraints depend on the specific type of 2HDM, we will present the complete analysis separately for each Yukawa type. This will allow us to conclude on the possible restrictions for the m_{12} values in the four 2HDM types.

5. Results

The results of our analysis are collected in Figs. 2, 3 and 4. In all the plots we show the \tilde{m} - m_{H^\pm} plane, where m_{12} is displayed at the top of each plot. The four columns in each of the figures represent the results in the four Yukawa types, correspondingly. The colored regions in these plots (except red, see below) correspond to the regions disallowed at the 2σ level by the “other constraints”: light gray regions are disallowed by the theoretical constraints, light blue regions are disallowed by LHC Higgs searches, yellow regions are disallowed by flavor observables (the two areas light blue and yellow together give the light green areas), dark gray regions are disallowed by the LHC rate measurements. It should be noted that light blue, yellow and green areas are only plotted inside the allowed region by the theoretical constraints and that the light gray areas in the lower right part of these plots are not clearly visible because they are hidden below the dark gray areas. The areas in white (disregarding red for now) represent the 2σ allowed regions by the previously called “other constraints”. On top of these allowed areas, we include the predicted allowed area by $\mu_{\gamma\gamma}$, which is displayed in red to be clearly distinguishable. These red veils with conical shape differentiate the 1σ allowed regions, see Eq. (9), which are limited by dotted lines and displayed in a darker red color, and the broader 2σ allowed regions, which are limited by dashed lines and displayed in a lighter red color. The solid red line is the contour line for $\mu_{\gamma\gamma}$ corresponding to the central experimental value. Notice that those red cones correspond to that shown in the lower left plot of Fig. 1. Following our description, the red shaded areas found on top of the areas that are allowed by the other constraints are in agreement with all experimental data. On the other hand, the areas that remain white after application of the $\mu_{\gamma\gamma}$ bounds marked in transparent red are the areas of our interest here in order to conclude on the additional constraints on m_{12} from $\mu_{\gamma\gamma}$. It is precisely these “reduced white regions” what define the final disallowed intervals in m_{12} that we are looking for.

The results in Figs. 2, 3 and 4 cover the three generic scenarios considered here that take into account the three qualitative different patterns of the BSM Higgs boson masses, which we classify and name accordingly by:

• Deg

This scenario sets all the BSM Higgs boson masses to be fully degenerate with: $m_A = m_H = m_{H^\pm}$. This is designed to easily evade the EWPO constraints.

• Par Deg

This scenario sets the BSM Higgs boson masses to be just partially degenerate with $m_A = m_{H^\pm}$ but m_H different. In this scenario we consider two different cases: 1) m_H fixed to a particular numerical value and 2) $m_H = \tilde{m}$. Again the dominant EWPO constraints from the T parameter are evaded.

• Split

This scenario is designed to possibly accommodate a new world average of m_W , including the recent CDF measurement [18]. In this scenario we consider non degenerate m_A , m_{H^\pm} and m_H . We set $m_A < m_{H^\pm}$, but with mass values m_A and m_{H^\pm} split by a fixed quantity Δm , as $m_A = m_{H^\pm} - \Delta m$. The other Higgs mass is set by: 1) m_H fixed to a particular numerical value, 2) $m_H = \tilde{m}$ and 3) $m_H = m_A$. We explore different values for the splitting between m_A and m_{H^\pm}

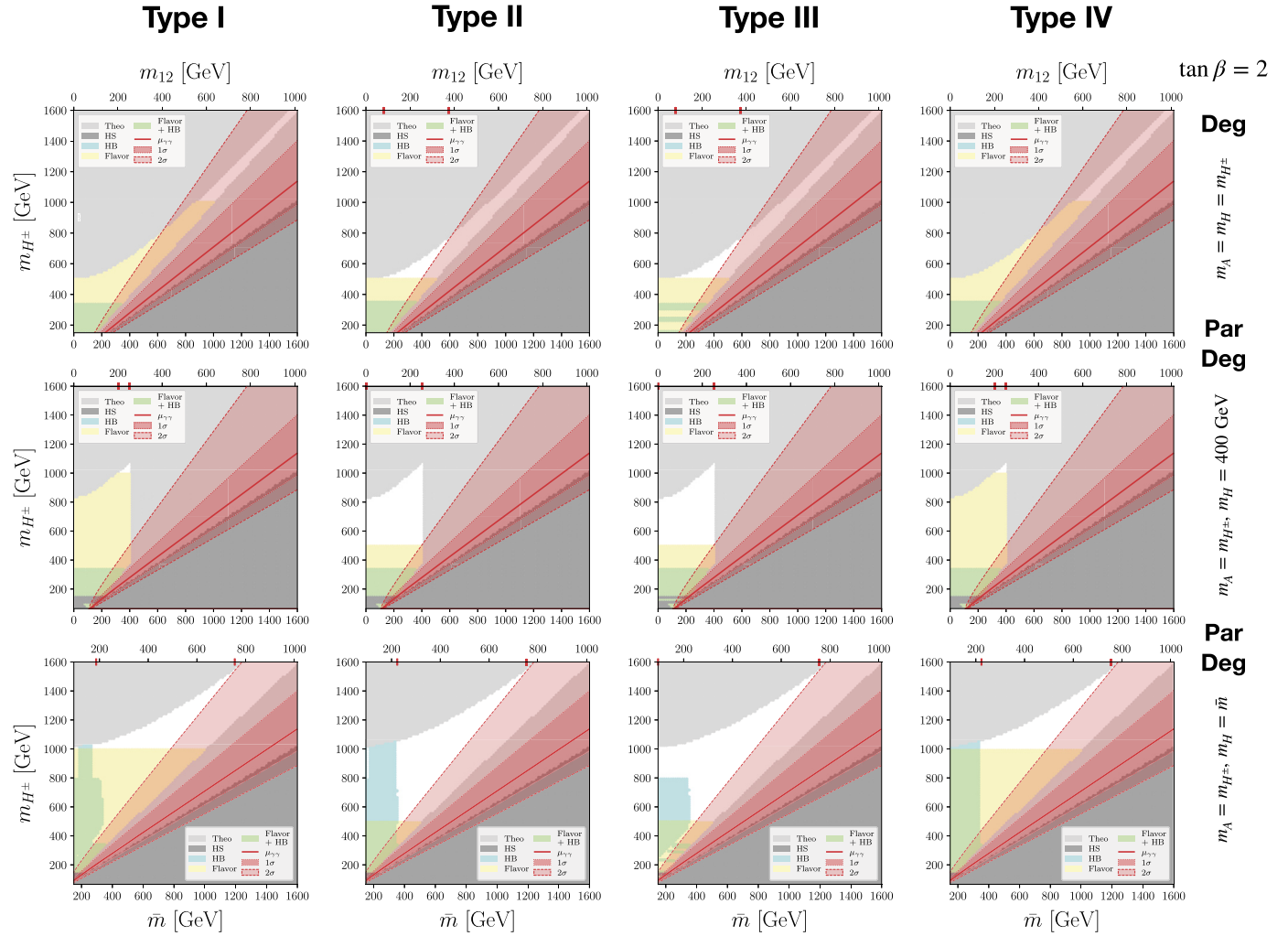


Fig. 2. Constraints in the four 2HDM types for the **Deg** and **Par Deg** cases with $\tan\beta = 2$ (see text).

and require that the value of m_W predicted in the 2HDM to be in agreement at the 2σ level with a possible new world average [4], including the recent CDF measurement [18], $m_W^{\text{exp,new}} \approx 80.417 \pm 0.018 \text{ GeV}$.² To calculate m_W in the 2HDM we use the one-loop approximation [17,32] given in terms of the S , T and U parameters,

$$m_W = m_W^{\text{SM}} \sqrt{1 + \frac{s_W^2}{c_W^2 - s_W^2} \Delta r'}, \quad \Delta r' = \frac{\alpha}{s_W^2} \left(-\frac{5}{2} + c_W^2 T + \frac{c_W^2 - s_W^2}{4s_W^2} U \right). \quad (11)$$

We take the numerical values for α , m_W^{SM} , $c_W^2 = 1 - s_W^2 = m_Z^2/m_Z^2$ from [4].

We start discussing the results in Fig. 2. In all plots in this figure we set $\tan\beta = 2$. In the first row the plots show the results for the scenario **Deg**, in the second row for the scenario **Par Deg** with $m_H = 400 \text{ GeV}$ and in the third row for the scenario **Par Deg** with $m_H = \bar{m}$. We first see that the patterns of the allowed areas by the theoretical constraints (i.e. the complementary areas to the light gray ones) are different in the three rows (but identical for the four Yukawa types, as required). In the scenario **Deg** these allowed areas appear as diagonal corridors whose widths get

narrower for larger values of $\tan\beta$ up to getting totally closed for about $\tan\beta > 10$ (not shown here). For more details on these corridors see Refs. [6,7]. The second row, for the **Par Deg** scenario with fixed $m_H = 400 \text{ GeV}$, shows that the allowed regions by the theoretical constraints are not corridors but they display rather as windows with sort of arrow tip shape placed at the lower left corner in these planes. In the third row, corresponding to the **Par Deg** case and setting $m_H = \bar{m}$, the allowed regions by the theoretical constraints display again as diagonal corridors, but wider in this scenario than in the **Deg** case. The dark gray areas are very similar in all the plots. The experimentally allowed/disallowed areas differentiating the most the four 2HDM types are the ones from flavor observables. The disallowed areas by flavor physics are very similar in type I and IV as well as in type II and III, see also the discussion in Ref. [7]. The total allowed areas by the “other constraints” are larger in type II and III than in type I and IV. Overlaid are the red areas allowed by $\mu_{\gamma\gamma}$, which are identical in all plots. Consequently, as discussed above, the “reduced white areas”, on the other hand, are excluded at the 2σ level by $\mu_{\gamma\gamma}$.

For the purpose of the present work, the most important conclusions from this figure are the following: 1) in all cases, all the regions that are allowed by all the other constraints are disallowed by $\mu_{\gamma\gamma}$ at the 1σ level; but, in contrast, 2) if we require compatibility with $\mu_{\gamma\gamma}$ at the 2σ level, there are some regions that are allowed by all the other constraints but are disallowed by $\mu_{\gamma\gamma}$ (the “reduced white areas”) (and some other regions that are allowed

² It should be noted that the values given so far in Ref. [4] are rather approximate.

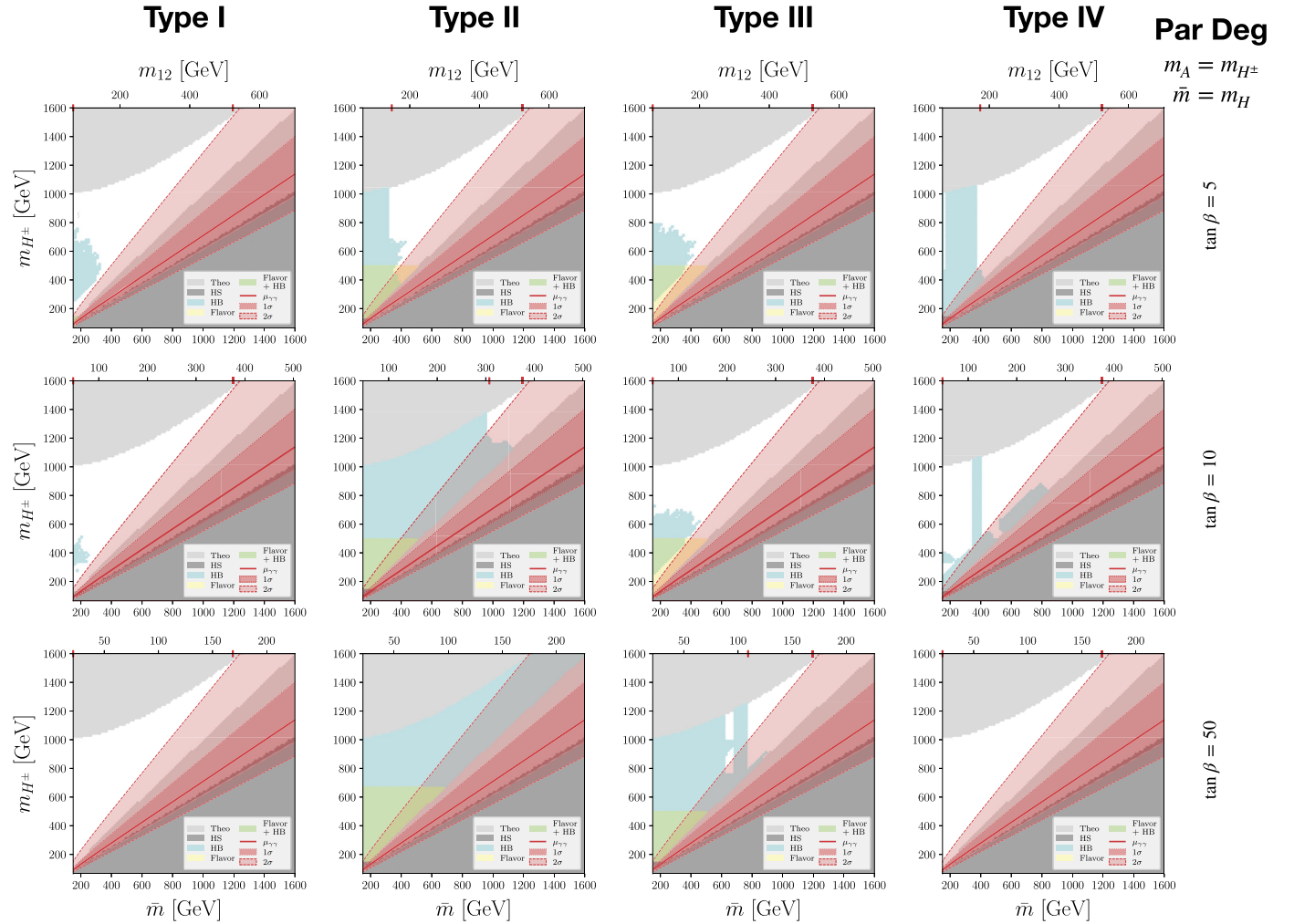


Fig. 3. Constraints in the four 2HDM types for the **Par Deg** case with $\tan\beta = 5, 10, 50$ (see text).

by both, the other constraints and $\mu_{\gamma\gamma}$). The “reduced white areas” appear in all the studied scenarios in this figure for type II and type III, and in the **Par Deg** scenarios for type I and IV. Therefore, the final constraints on m_{12} can be extracted from the interval that is projected on the top axis of these plots from the “reduced white regions” and the intercept with the red region, that are marked in the figures with red ticks in the upper axis. Thus, in the three scenarios analyzed, for $\tan\beta = 2$ and $c_{\beta-\alpha} = 0$ we get the following disallowed intervals in m_{12} by $\mu_{\gamma\gamma}$: [81, 374] GeV in type II and III for the **Deg** case; [202, 253] GeV in type I and IV, and [0, 253] GeV in type II and III for the **Par Deg** case with $m_H = 400$ GeV; and [186, 755] GeV in type I, [223, 755] GeV in type II, [0, 755] GeV in type III and [95, 253] GeV in type IV for the **Par Deg** case with $m_H = \tilde{m}$.

Next we discuss the results of Fig. 3, where we explore the scenario **Par Deg** with $m_H = \tilde{m}$ for different values of $\tan\beta = 5, 10, 50$ in the upper, middle and lower row, respectively. We have not explored values of $\tan\beta > 2$ in the other two scenarios because the theoretical constraints effectively close the allowed area. The red areas, displaying the regions allowed by $\mu_{\gamma\gamma}$ are by construction the same and identical to Fig. 2. In this figure there are regions allowed by the “other constraints” in all the plots (except in type II for $\tan\beta = 50$), and consequently one can extract constraints on m_{12} from all of them. The regions allowed by the “other constraints” are wider than in the previous figure. As before the pattern of these regions are more similar in the type I and IV as well as in type II and III. Since we have related in this figure m_{12}

to m_H via the setting $m_H = \tilde{m}$, not all the derived constraints on m_{12} appear to come from $\mu_{\gamma\gamma}$ but instead from the other constraints. However, this implies really limitations on m_H , and not on m_{12} . For instance, the value $m_{12} = 0$ is not included in this figure (whereas, it did appear in some of the plots in the previous figure) since a very light m_H is never allowed by the collider constraints and, furthermore, by definition $m_H > m_h \sim 125$ GeV. In summary, for the scenario **Par Deg** and $m_H = \tilde{m}$ we get the following disallowed intervals in m_{12} by $\mu_{\gamma\gamma}$: [66, 523] GeV in type I and type III, [148, 523] GeV in type II and [174, 523] GeV in type IV for $\tan\beta = 5$; [47, 376] GeV in type I, III and IV and [307, 376] GeV in type II for $\tan\beta = 10$; and [21, 169] GeV in type I and IV, [109, 169] GeV in type III for $\tan\beta = 50$.

Finally, we discuss the results in Fig. 4. These explore the scenario with split m_{H^\pm} and m_A values, such that $m_A = m_{H^\pm} - \Delta m$. We have set $\tan\beta = 2$ in this figure and present three cases in which we find agreement with a possible new world average $m_W^{\text{exp,new}}$ at the 2σ level.³ The disallowed areas by m_W are shown in these plots by the striped regions, which by construction are identical in all four Yukawa types. In the first row we set $\Delta m = 100$ GeV and $m_H = m_A$, in the second row $\Delta m = 20$ GeV and $m_H = 400$ GeV, and in the third row $\Delta m = 20$ GeV and $m_H = \tilde{m}$. We see in the first row that $m_W^{\text{exp,new}}$ yields no additional con-

³ Analysis in the 2HDM taking into account the recent CDF measurement of m_W can be found, e.g., in Refs. [33–35].

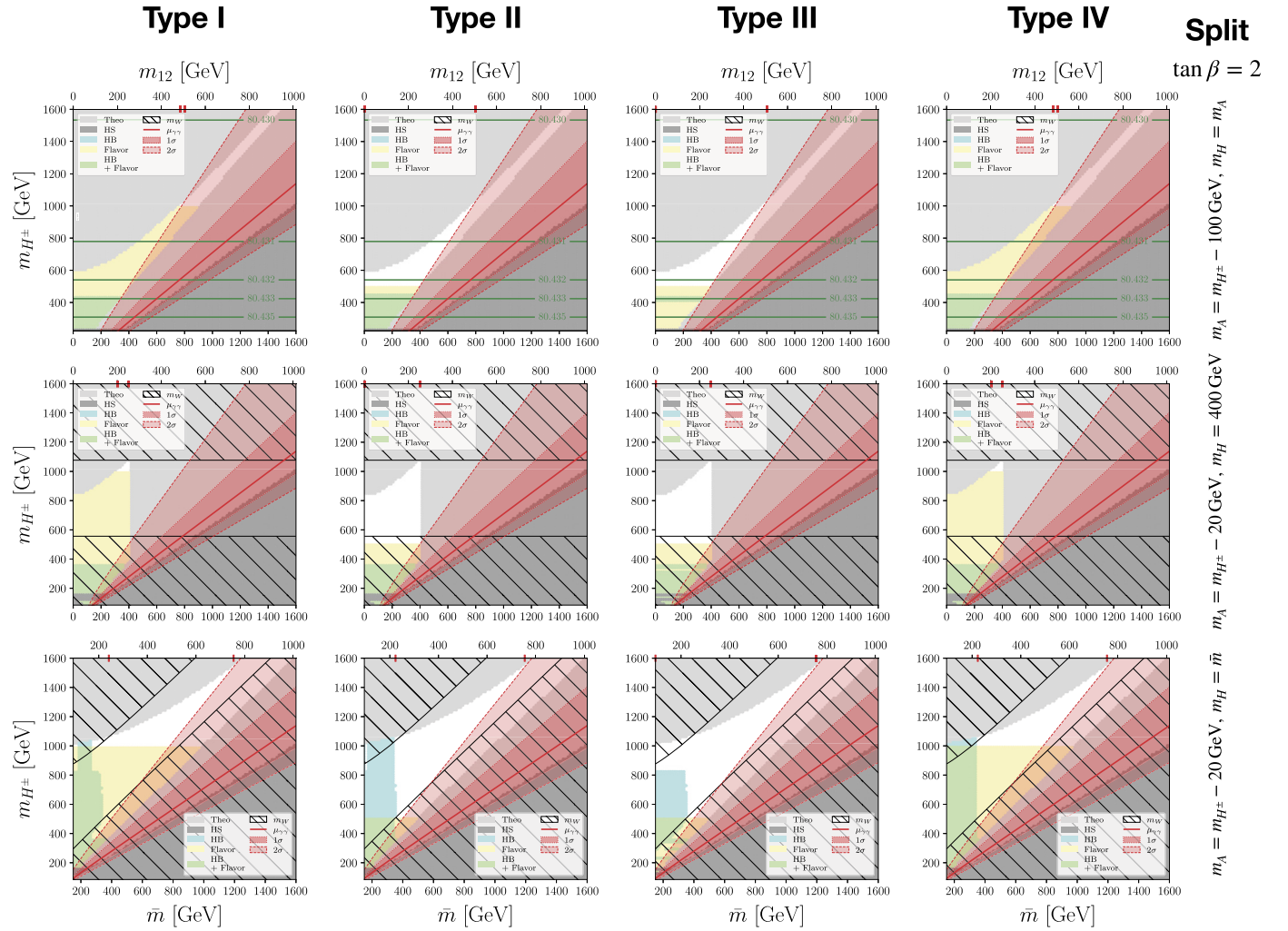


Fig. 4. Constraints in the four 2HDM types for the **Split** case with $\tan \beta = 2$ (see text).

straints, i.e. no striped region appears. In fact, the specified horizontal contour lines with the predicted m_W in the 2HDM are all compatible with $m_W^{\text{exp,new}}$ within 2σ . Therefore, the conclusions on the m_{12} constraints are very similar to the fully degenerate case of Fig. 2. Other choices for Δm in the interval $[60, 110]$ GeV with $m_H = m_A$ yield a similar result for the regions allowed by the “other constraints”. Δm values outside this interval do not exhibit allowed regions by $m_W^{\text{exp,new}}$ and result in a fully striped plots. In the second row we have chosen $\Delta m = 20$ GeV and $m_H = 400$ GeV. In this case the parameter space allowed by $m_W^{\text{exp,new}}$ is a horizontal band from $m_{H^\pm} = 572$ GeV to $m_{H^\pm} = 1062$ GeV. Since this band contains almost all the region allowed by all the other constraints, the conclusions on the final constraints on m_{12} are very similar to results found in the second row of Fig. 2. In the third row we set $\Delta m = 20$ GeV and $m_H = \tilde{m}$. This results in a diagonal band allowed by $m_W^{\text{exp,new}}$, going from low values of \tilde{m} , m_{H^\pm} to large values of these parameters. The intersection between this diagonal band and the “reduced white area” provides the joint allowed region. The projection of this final allowed region on to the upper axis and the intercept with the red region provides the wanted constraints on m_{12} . This gives the following disallowed intervals: $[486, 506]$ GeV in type I and IV and $[0, 506]$ GeV in type II and III for $\Delta m = 100$ GeV and $m_H = m_A$; $[202, 253]$ GeV in type I and IV and $[0, 253]$ GeV in type II and III for $\Delta m = 20$ GeV and $m_H = 400$ GeV; and $[242, 755]$ GeV in type I, $[223, 755]$ GeV in

type II and IV and $[94, 755]$ GeV in type III for $\Delta m = 20$ GeV and $m_H = \tilde{m}$.

6. Conclusions

In the present paper we have analyzed possible constraints on the Z_2 soft-breaking parameter m_{12} in the 2HDM, where we have focused on the alignment limit, we have demonstrated that it is possible to obtain constraints on m_{12} from the comparison of the theoretical prediction of $\text{BR}(h \rightarrow \gamma\gamma)$ with the present data on the di-photon signal strength. The results of these constraints are summarized in Figs. 2, 3 and 4. The new intervals of m_{12} that are disallowed at 2σ by $\mu_{\gamma\gamma}$ while being allowed by all the other constraints have been derived for the four 2HDM types, in several scenarios for the heavy Higgs boson masses, as summarized in the previous section. In particular we find that taking into account the new measurement of m_W^{CDF} has only a mild impact on the derived limits on m_{12} .

Declaration of competing interest

The authors declare that they have no known competing financial interests or personal relationships that could have appeared to influence the work reported in this paper.

Data availability

The data that has been used is confidential.

Acknowledgements

The present work has received financial support: from the grant IFT Centro de Excelencia Severo Ochoa CEX2020-001007-S funded by MCIN/AEI/10.13039/501100011033; from the grant PID2019-110058GB-C21 funded by MCIN/AEI/10.13039/501100011033 and by “ERDF A way of making Europe”; from the MCIN via the Spanish “Agencia Estatal de Investigación” (AEI) and the EU “Fondo Europeo de Desarrollo Regional” (FEDER) through the project PID2019-108892RB-I00/AEI/10.13039/501100011033; from the European Union’s Horizon 2020 research and innovation programme under the Marie Skłodowska-Curie grant agreement No. 674896 and No. 860881-HIDDeN; and from the MCIN via the FPU grant with code FPU18/06634.

References

- [1] J.F. Gunion, H.E. Haber, G.L. Kane, S. Dawson, *Front. Phys.* **80** (2000) 1–404, SCIPP-89/13, Erratum: arXiv:hep-ph/9302272.
- [2] M. Aoki, S. Kanemura, K. Tsumura, K. Yagyu, *Phys. Rev. D* **80** (2009) 015017, arXiv:0902.4665 [hep-ph].
- [3] G.C. Branco, P.M. Ferreira, L. Lavoura, M.N. Rebelo, M. Sher, J.P. Silva, *Phys. Rep.* **516** (2012) 1, arXiv:1106.0034 [hep-ph].
- [4] R.L. Workman, et al., *Particle Data Group*, *PTEP* **2022** (2022) 083C01.
- [5] S.L. Glashow, S. Weinberg, *Phys. Rev. D* **15** (1977) 1958.
- [6] F. Arco, S. Heinemeyer, M.J. Herrero, *Eur. Phys. J. C* **80** (9) (2020) 884, arXiv:2005.10576 [hep-ph].
- [7] F. Arco, S. Heinemeyer, M.J. Herrero, *Eur. Phys. J. C* **82** (6) (2022) 536, arXiv:2203.12684 [hep-ph].
- [8] F. Arco, S. Heinemeyer, M.J. Herrero, *Eur. Phys. J. C* **81** (10) (2021) 913, arXiv:2106.11105 [hep-ph].
- [9] J.R. Ellis, M.K. Gaillard, D.V. Nanopoulos, *Nucl. Phys. B* **106** (1976) 292.
- [10] M.A. Shifman, A.I. Vainshtein, M.B. Voloshin, V.I. Zakharov, *Sov. J. Nucl. Phys.* **30** (1979) 711–716, ITEP-42-1979.
- [11] J. Bernal, J.F. Gunion, H.E. Haber, Y. Jiang, S. Kraml, *Phys. Rev. D* **92** (7) (2015) 075004, arXiv:1507.00933 [hep-ph].
- [12] D. Eriksson, J. Rathsmann, O. Stål, *Comput. Phys. Commun.* **181** (2010) 189, arXiv:0902.0851 [hep-ph].
- [13] A. Arhrib, M. Capdequi Peyranere, W. Hollik, S. Penaranda, *Phys. Lett. B* **579** (2004) 361–370, arXiv:hep-ph/0307391 [hep-ph].
- [14] M.E. Peskin, T. Takeuchi, *Phys. Rev. Lett.* **65** (1990) 964.
- [15] M.E. Peskin, T. Takeuchi, *Phys. Rev. D* **46** (1992) 381.
- [16] W. Grimus, L. Lavoura, O.M. Ogreid, P. Osland, *J. Phys. G* **35** (2008) 075001, arXiv:0711.4022 [hep-ph].
- [17] W. Grimus, L. Lavoura, O.M. Ogreid, P. Osland, *Nucl. Phys. B* **801** (2008) 81–96, arXiv:0802.4353 [hep-ph].
- [18] T. Aaltonen, et al., *CDF, Science* **376** (6589) (2022) 170–176.
- [19] G. Bhattacharyya, D. Das, *Pramana* **87** (3) (2016) 40, arXiv:1507.06424 [hep-ph].
- [20] P. Bechtle, O. Brein, S. Heinemeyer, G. Weiglein, K.E. Williams, *Comput. Phys. Commun.* **181** (2010) 138, arXiv:0811.4169 [hep-ph].
- [21] P. Bechtle, D. Dercks, S. Heinemeyer, T. Klingl, T. Stefaniak, G. Weiglein, J. Wittbrodt, arXiv:2006.06007 [hep-ph].
- [22] P. Bechtle, S. Heinemeyer, O. Stål, T. Stefaniak, G. Weiglein, *Eur. Phys. J. C* **74** (2) (2014) 2711, arXiv:1305.1933 [hep-ph].
- [23] P. Bechtle, S. Heinemeyer, T. Klingl, T. Stefaniak, G. Weiglein, J. Wittbrodt, *Eur. Phys. J. C* **81** (2) (2021) 145, arXiv:2012.09197 [hep-ph].
- [24] T. Enomoto, R. Watanabe, *J. High Energy Phys.* **1605** (2016) 002, arXiv:1511.05066 [hep-ph].
- [25] A. Arbey, F. Mahmoudi, O. Stål, T. Stefaniak, *Eur. Phys. J. C* **78** (3) (2018) 182, arXiv:1706.07414 [hep-ph].
- [26] T. Abe, R. Sato, K. Yagyu, *J. High Energy Phys.* **07** (2015) 064, arXiv:1504.07059 [hep-ph].
- [27] F. Mahmoudi, *Comput. Phys. Commun.* **180** (2009) 1579, arXiv:0808.3144 [hep-ph].
- [28] F. Mahmoudi, *Comput. Phys. Commun.* **180** (2009) 1718–1719.
- [29] M. Misiak, A. Rehman, M. Steinhauser, *J. High Energy Phys.* **06** (2020) 175, arXiv:2002.01548 [hep-ph].
- [30] P. Arnan, D. Becirevic, F. Mescia, O. Sumensari, *Eur. Phys. J. C* **77** (11) (2017) 796, arXiv:1703.03426 [hep-ph].
- [31] S. Hossenberger, W. Hollik, arXiv:2207.03845 [hep-ph].
- [32] T. Biekötter, S. Heinemeyer, G. Weiglein, arXiv:2204.05975 [hep-ph].
- [33] H. Song, W. Su, M. Zhang, arXiv:2204.05085 [hep-ph].
- [34] H. Bahl, J. Braathen, G. Weiglein, arXiv:2204.05269 [hep-ph].
- [35] K.S. Babu, S. Jana, P.K. Vishnu, arXiv:2204.05303 [hep-ph].